Letter

Imaging the interface of a qubit and its quantum-many-body environment

S. Rammohan,[1,*] S. Tiwari,[1] A. Mishra,[1] A. Pendse,[1] A. K. Chauhan,[1,2] R. Nath,[3] A. Eisfeld,[4] and S. Wüster[1,†]

[1]*Department of Physics, Indian Institute of Science Education and Research, Bhopal, Madhya Pradesh 462 066, India*

[2]*Department of Optics, Faculty of Science, Palacký University, 17. listopadu 1192/12, 77146 Olomouc, Czech Republic*

[3]*Department of Physics, Indian Institute of Science Education and Research, Pune 411 008, India*

[4]*Max Planck Institute for the Physics of Complex Systems, Nöthnitzer Strasse 38, 01187 Dresden, Germany*

(Received 22 November 2020; revised 6 January 2021; accepted 2 November 2021; published 23 December 2021)

Decoherence affects all quantum systems, natural or artificial, and is the primary obstacle impeding quantum technologies. We show theoretically that for a Rydberg qubit in a Bose condensed environment, experiments can image the system-environment interface that is central for decoherence. High-precision absorption images of the condensed environment will be able to capture transient signals that show the real-time buildup of a mesoscopic entangled state in the environment. This is possible before decoherence sources other than the condensate itself can kick in, since qubit decoherence timescales can be tuned from the order of nanoseconds to microseconds by a choice of the excited Rydberg principal quantum number ν. Imaging the interface will allow detailed explorations of open quantum system concepts and may offer guidance for coherence protection in challenging scenarios with non-Markovian environments.

DOI: 10.1103/PhysRevA.104.L060202

Introduction. Quantum decoherence [1,2] is central to quantum science and technologies, for which it mainly represents an obstacle but also is increasingly considered a possible resource [3–5]. Decoherence also often reconciles our everyday experience with the laws of quantum mechanics, explaining the gradual loss of interference features once a hitherto isolated quantum object begins to interact with its environment. The cause is not a reluctance of the macroscopic environment to participate in nonclassical aspects of quantum physics such as superposition states, but its propensity to entangle with every microscopic system interacting with it.

This entanglement diminishes interference features involving the quantum object, to the point where they become unobservable. Experiments are typically confined to measurements of the quantum object, since it is difficult to extract useful information about a large and complex environment. Here, we propose an exceptional platform where crucial parts of the environment around a qubit can also be probed. We show that exciting an impurity atom in a Bose-Einstein condensate (BEC) to Rydberg states [6–14] provides a scenario where the reduced dynamics of the Rydberg [15,16] qubit and the evolution of its environment are both observable. Even the buildup of mesoscopic entanglement during the decoherence time can be probed.

This direct window on the interface between a qubit and its environment is enabled by the extraordinary properties of Rydberg atoms and BEC. First, the atom can simultaneously interact with a large portion of the environment due to the wide excursions of its electron [9], providing interaction ranges of about 1 μm. Second, the many-body quantum state of the BEC environment can be well approximated by a quite simple product ansatz [17] that nonetheless describes a large number of atoms. This allows the observation of the BEC evolution while decoherence of the Rydberg system takes place.

Probing the environment while it is causing decoherence would be significantly more challenging around ground-state qubits, on which earlier work regarding the decoherence of impurity atoms within a BEC has focused [18–28]. Due to the much shorter interaction range, ∼nm in this case, one would have to resort to indirect methods [29], involving high-precision quasiparticle spectroscopy [30], that can only

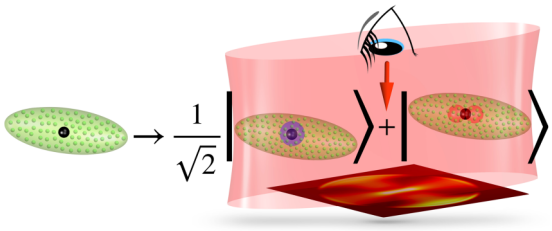

FIG. 1. Imaging the environmental origin of decoherence. Left: We assume a distinct impurity atom (dark spot) is embedded at the center of the BEC (green ellipsoid) of ground-state atoms (green balls). Right: The impurity is rapidly transferred into a coherent superposition of two different electronic Rydberg states, $|s\rangle$ (blue shade) and $|p\rangle$ (orange shade), forming a qubit. In either state the electron makes large excursions into the ambient BEC medium, within the orbital volume indicated by the blue and orange shaded areas. In this volume, the electron will imprint a phase pattern onto the coherent condensate wave function, entangling it with the qubit. Due to the well-controlled and coherent environmental initial state, this entangled pattern can be imaged (bottom, red laser beam).

*sidharth16@iiserb.ac.in

†sebastian@iiserb.ac.in

interrogate the environment with some delay. Also in cavity QED, which has provided some of the most direct observations of decoherence dynamics [31–33], it would be a major challenge to interrogate the system and environment in the same experiment.

Our qubit state is a superposition $|\chi\rangle = c_\downarrow|s\rangle + c_\uparrow|p\rangle$ of angular momentum states $|s\rangle = |\nu(l=0)\rangle \equiv |\downarrow\rangle$ and $|p\rangle = |\nu(l=1, m=0)\rangle \equiv |\uparrow\rangle$, for a Rydberg atom with a large principal quantum number (e.g., $\nu = 80$), created in a BEC of N atoms. In either state, hundreds of condensate atoms are located within the Rydberg electron orbit (see Fig. 1). Interactions of these atoms with the electron then imprint a macroscopic phase pattern onto the condensate [34]. Crucially, this pattern is different for different electronic states [35], hence the condensate environment entangles with the Rydberg qubit, causing decoherence of the latter.

We will demonstrate that the proposed platform is exceptionally well suited to interrogate the intertwined dynamics of the qubit and its environment that leads to deocherence: (i) Qubit decoherence is accessible by Ramsey microwave interferometry [36–38]. (ii) Absorption images show the transient buildup of the mesoscopically entangled state causing decoherence. (iii) Non-Markovian quantum-many-body dynamics can be accessed, where observations will challenge the best numerical techniques available. Such studies can provide insight into avoiding decoherence or exploiting it for quantum technologies [3–5].

Interactions between qubit and environment. We have shown in Ref. [39], starting from the many-body Hamiltonian, that the electronic dynamics of the Rydberg impurity embedded in the BEC is described in the Bogoliubov approximation by the spin-boson model [40–44] (SBM) $\hat{H}_{\rm tot} = \hat{H}_{\rm syst} + \hat{H}_{\rm env} + \hat{H}_{\rm int}$, in terms of the Rydberg pseudospin defined earlier, with

$$\hat{H}_{\rm syst} = \frac{\hbar\Omega_{\rm mw}}{2}\hat{\sigma}_x + \frac{\Delta E(t)}{2}\hat{\sigma}_z, \quad \hat{H}_{\rm env} = \sum_{\mathbf{q}} \hbar\omega_{\mathbf{q}}\, \tilde{b}^\dagger_{\mathbf{q}}\tilde{b}_{\mathbf{q}},$$

$$\hat{H}_{\rm int} = \sum_{\mathbf{q}} \frac{\Delta\kappa^-_{\mathbf{q}}}{2}(\tilde{b}_{\mathbf{q}} + \tilde{b}^\dagger_{\mathbf{q}})\hat{\sigma}_z. \tag{1}$$

The $\hat{\sigma}_k$ are Pauli operators and the operators $\tilde{b}_{\mathbf{q}}$ destroy Bogoliubov–de Gennes (BdG) excitations with wave vector $\mathbf{q}$. Further, $\Omega_{\rm mw}$ is the Rabi frequency of the microwave coupling between the $|p\rangle$ and $|s\rangle$ Rydberg state, with $\Delta E(t) = \Delta + \bar{E}(t)$, where Δ is the effective energy splitting without the small time-dependent shift $\bar{E}(t)$ due to the environment [39]. The BdG mode energies are $\hbar\omega_q = \sqrt{E_q(E_q + U_0\rho)}$, with $q = |\mathbf{q}|$ and $E_q = \hbar^2q^2/2m$ for a homogeneous condensate of atoms with mass m at density ρ and interaction strength U_0. Finally, the coupling strengths to BdG modes are [39]

$$\Delta\kappa^\pm_{\mathbf{q}} = g_0\sqrt{\rho}\int d^3\mathbf{x}\left(\left|\psi^{(p)}(\mathbf{x})\right|^2 \pm \left|\psi^{(s)}(\mathbf{x})\right|^2\right) \times [u_{\mathbf{q}}(\mathbf{x}) - v^*_{\mathbf{q}}(\mathbf{x})], \tag{2}$$

where g_0 is the strength of electron-atom interactions [45,46], $\psi^{(\alpha)}(\mathbf{x})$ the Rydberg electron wave function in state α, and $u_{\mathbf{q}}(\mathbf{x}) = \frac{\bar{u}_{\mathbf{q}}}{\sqrt{\mathcal{V}}}e^{i\mathbf{q}\mathbf{x}}$, $v_{\mathbf{q}}(\mathbf{x}) = \frac{\bar{v}_{\mathbf{q}}}{\sqrt{\mathcal{V}}}e^{i\mathbf{q}\mathbf{x}}$ are BdG mode functions. $\mathcal{V}$ is the quantization volume, and $\bar{u}_{\mathbf{q}}$, $\bar{v}_{\mathbf{q}}$ are BdG amplitudes [17]. The system-environment coupling $\Delta\kappa^-_{\mathbf{q}}$ originates from contact interactions between the Rydberg electron and the ground-state atoms. The electronic state dependence is encapsulated by the term in parentheses, which thus governs the strength of the system-environment coupling.

Qubit decoherence. As a prelude to interface imaging in the next section, we first focus on decoherence of the qubit itself to predict decoherence timescales. These will turn out highly tunable, which will be essential for practical implementations. To estimate the decoherence timescale, it is sufficient to consider the simple scenario when there is no coupling between the two spin states, implying $\Omega_{\rm mw} = 0$. Thus, while we assume a chirped microwave is adiabatically followed to create the superposition qubit state $|\chi\rangle$ with $c_\downarrow = c_\uparrow = 1/\sqrt{2}$, which we call $|+\rangle$, the microwave should then subsequently be switched off.

We can hence study the Hamiltonian $\hat{H}_{\rm tot}$ with $\Omega_{\rm mw} = 0$ and $\Delta = E_p - E_s$, the energy difference between the Rydberg states. The many-body Hamiltonian then decomposes into blocks $\hat{H}_{\rm tot} = |\uparrow\rangle\langle\uparrow| \otimes \hat{H}_{{\rm ph},\uparrow} + |\downarrow\rangle\langle\downarrow| \otimes \hat{H}_{{\rm ph},\downarrow}$, where $\hat{H}_{{\rm ph},\downarrow/\uparrow}$ pertain to the environment (phonon) space only. Hence also the time evolution can be separately found in each of those blocks, yielding a global time-evolution operator $\hat{U} = |\uparrow\rangle\langle\uparrow| \otimes \hat{U}_{{\rm ph},\uparrow} + |\downarrow\rangle\langle\downarrow| \otimes \hat{U}_{{\rm ph},\downarrow}$, where $\hat{U}_{{\rm ph},\uparrow}$ ($\hat{U}_{{\rm ph},\downarrow}$) denotes a unitary operator that acts on BdG modes only, for the case where the system is in the $|\uparrow\rangle$ ($|\downarrow\rangle$) state. The above $\hat{U}$ implies a time-evolved state

$$|\Psi_{\rm tot}(t)\rangle = c_\uparrow|\uparrow\rangle \otimes |\Psi_\uparrow(t)\rangle + c_\downarrow|\downarrow\rangle \otimes |\Psi_\downarrow(t)\rangle. \tag{3}$$

States labeled Ψ are quantum-many-body states. In (3), $|\Psi_{\rm tot}(t)\rangle$ includes the qubit while $|\Psi_{\uparrow,\downarrow}(t)\rangle$ describes only the environment. For a state of the bipartite form (3), the coherence between $|\uparrow\rangle$ and $|\downarrow\rangle$ in the reduced density matrix for the qubit is

$$\rho_{\downarrow\uparrow}(t) = c^*_\downarrow c_\uparrow \langle\Psi_\uparrow(t)|\Psi_\downarrow(t)\rangle. \tag{4}$$

We will refer to $|r(t)| = |\langle\Psi_\uparrow(t)|\Psi_\downarrow(t)\rangle|$ as the coherence factor, which quantifies the distinguishability of the environmental states entangled with the spin [1,2]. It can be evaluated explicitly from the total time evolution operator $\hat{U}(t) = \mathcal{T}\exp[-\frac{i}{\hbar}\int_0^t \hat{H}'_{\rm int}(t')\,dt']$ of the SBM, where $\hat{H}'_{\rm int}$ denotes $\hat{H}_{\rm int}$ in the interaction picture. The two blocks discussed above are then

$$\hat{U}_{{\rm ph},\alpha}(t) = \exp\left[\alpha\sum_{\mathbf{q}}\frac{\Delta\kappa^-_{\mathbf{q}}}{\hbar\omega_{\mathbf{q}}}\left[\tilde{b}_{\mathbf{q}}(0)(e^{-i\omega_{\mathbf{q}}t} - 1) - \tilde{b}^\dagger_{\mathbf{q}}(0)(e^{i\omega_{\mathbf{q}}t} - 1)\right]\right], \tag{5}$$

with $\alpha \in \{-\frac{1}{2}, \frac{1}{2}\} \leftrightarrow \{\downarrow, \uparrow\}$. In the Bogoliubov vacuum we then find $r(t) = \langle 0|\hat{U}^\dagger_{{\rm ph},\uparrow}(t)\hat{U}_{{\rm ph},\downarrow}(t)|0\rangle$, which yields

$$r(t) = \exp\left[-\sum_{\mathbf{q}}\left(\frac{\Delta\kappa^-_{\mathbf{q}}}{\hbar\omega_{\mathbf{q}}}\right)^2[1 - \cos(\omega_{\mathbf{q}}t)]\right]. \tag{6}$$

For short times, we can approximate

$$|r(t)| \approx e^{-(t/T_{\rm dc})^2}, \quad T_{\rm dc} = \left(\sum_{\mathbf{q}} (\Delta\kappa_{\mathbf{q}}^{-})^2/(2\hbar^2)\right)^{-1/2}, \quad (7)$$

with a decoherence timescale $T_{\rm dc}$. Exploiting the framework setup in Ref. [39], we find from (7) that $T_{\rm dc}$ can be tuned from $T_{\rm dc} \approx 20$ ns at $\nu = 40$ to $T_{\rm dc} \approx 1$ μs at $\nu = 120$ through a choice of principal quantum number ν, while other parameters are given in Ref. [46]. The coherence evolution $|r(t)|$ of the Rydberg impurity is measurable with microwave Ramsey interferometry [36–38]. For most $T_{\rm dc}$ above, the process described will be faster than other decoherence sources, such as blackbody radiation [47], phonon-phonon interactions [48], atomic losses [49–51], or spontaneous decay [52]. Since Eq. (7) depends on the microscopic interactions between Rydberg and BEC atoms, decoherence measurements will open an additional route to understand these.

Extracting decoherence from environmental mean-field dynamics. Spin coherence is intimately linked to the dynamics of the environment through Eq. (4). We now show that the extreme coherence of the BEC environment allows experimental imaging of this joint dynamics, and the prediction of the expected signature in a simple case. The block decomposition of the many-body Hamiltonian for $\Omega_{\rm mw} = 0$ suggests to use the mean-field Gross-Pitaevskii equation (GPE) for each block separately. Decoherence of the superposition is then captured by the overlap of these individual condensate mean-field solutions. We thus write the many-body wave function for the Bose gas as $\langle \mathbf{X}|\Psi_\alpha(t)\rangle = \prod_k^N \varphi_\alpha(\mathbf{x}_k)$, for $\alpha \in \{\uparrow, \downarrow\}$, where $\mathbf{X} \in \mathbb{R}^{3N}$ groups all atomic positions, while $\mathbf{x}_k$ are those of atom k only. Thus for a fixed Rydberg state α, all ground-state atoms are in the same single-particle state $|\varphi_\alpha\rangle$, while through Eq. (3) this single-particle state is entangled with the impurity state. If there is an impurity in the state $|\alpha\rangle$ located at $\mathbf{r} = \mathbf{0}$, the three-dimensional (3D) GPE reads [12,34,35,54,55]

$$i\hbar\frac{\partial}{\partial t}\phi_\alpha = \left(-\frac{\hbar^2}{2m}\nabla^2 + U_0|\phi_\alpha|^2 + g_0\left|\psi^{(\alpha)}\right|^2\right)\phi_\alpha, \quad (8)$$

where $\psi^{(\alpha)} = \psi^{(\alpha)}(\mathbf{r})$ is the Rydberg electron wave function of the impurity and $\phi_\alpha = \phi_\alpha(\mathbf{r}) = \sqrt{N}\varphi_\alpha(\mathbf{r})$ the BEC mean-field wave function.

With the separate mean-field ansatz for each impurity state discussed above, the coherence factor becomes

$$|r_{\rm GPE}(t)| = \left|\left(\int d^3\mathbf{r}\, \phi_\uparrow^*(\mathbf{r})\phi_\downarrow(\mathbf{r})/N\right)^N\right|. \quad (9)$$

We now show that (9) and (7) ought to agree for short times. The evolution of an initially homogeneous condensate mean field for short times and dominant $g_0|\psi^{(\alpha)}(\mathbf{x})|$ can be found directly from Eq. (8) as

$$\phi_\alpha(\mathbf{x}, t) = \sqrt{\rho}\left(1 - \frac{i}{\hbar}g_0\left|\psi^{(\alpha)}(\mathbf{x})\right|^2 t\right). \quad (10)$$

This is exactly reproduced by the SBM. To see this, we write the mean-field wave function as $\phi(\mathbf{x}, t) = \langle\hat{\Psi}(\mathbf{x}, t)\rangle$, where

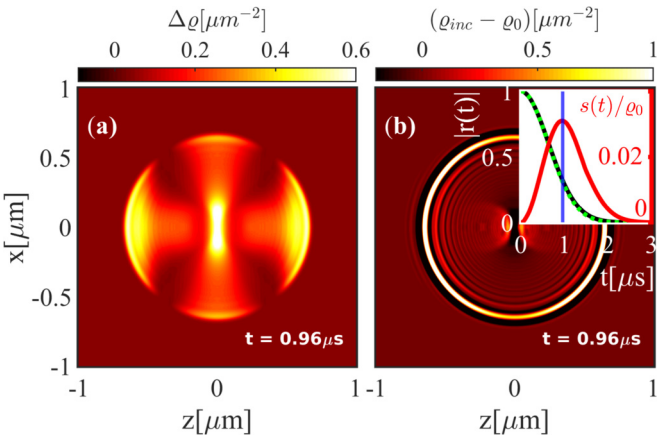

FIG. 2. Interface imaging. (a) The column density difference $\overline{\Delta\varrho}$ from the total density difference $\Delta\varrho = \varrho_{\rm ms}(\mathbf{r}) - \varrho_{\rm inc}(\mathbf{r})$ in Eq. (16) between two scenarios, where $\varrho_{\rm inc} = (\varrho_\uparrow + \varrho_\downarrow)/2$ is an incoherent mixture of the patterns imprinted by a $|s\rangle = |\downarrow\rangle$ or $|p\rangle = |\uparrow\rangle$ Rydberg state at $\nu = 80$, while for $\varrho_{\rm ms}$ the BEC is in a mesoscopic superposition of these two patterns. See also the movie in the Supplemental Material [53], and parameters in Ref. [46]. (b) As a reference we show $\overline{\varrho_{\rm inc}}$ alone, relative to the background value $\varrho_0 = 24.1$ μm^{-2}. The inset shows the Rydberg coherence factor $|r(t)|$ between $|s\rangle$ and $|p\rangle$, with $|r(t)|$ from the SBM in Eq. (7) (green dotted), from the GPE orbital overlap in Eq. (9) (black), and the spatial maximum $s(t) = \max_{x,z}\overline{\Delta\varrho}(x, z, t)$ (red solid line) peaking at $t = 0.96$ μs used in (a) and (b) (blue vertical line).

the bosonic field operator is

$$\hat{\Psi}(\mathbf{x}, t) = \sqrt{\rho} + \sum_{\mathbf{q}}\left[u_{\mathbf{q}}(\mathbf{x})(\tilde{b}_{\mathbf{q}}(t) - d_{\mathbf{q}}) - v_{\mathbf{q}}^*(\mathbf{x})(\tilde{b}_{\mathbf{q}}^\dagger(t) - d_{\mathbf{q}}^*)\right], \quad (11)$$

based on shifted BdG modes for which the initial state $|\boldsymbol{d}\rangle$ is a many-mode coherent state $\tilde{b}_{\mathbf{q}}|\boldsymbol{d}\rangle = d_{\mathbf{q}}|\boldsymbol{d}\rangle$, with offset $d_{\mathbf{q}} = \frac{\Delta\kappa_{\mathbf{q}}^{+}}{2\hbar\omega_{\mathbf{q}}}$. The offset arises through the sudden insertion of the Rydberg impurity at $t = 0$ [39]. We then use Eq. (11) and evaluate,

$$\phi_\alpha(\mathbf{x}, t) = \langle\alpha|\langle\boldsymbol{d}|\,\hat{U}_{{\rm ph},\alpha}^\dagger(t)\hat{\Psi}(t)\hat{U}_{{\rm ph},\alpha}(t)\,|\alpha\rangle|\boldsymbol{d}\rangle, \quad (12)$$

where the subscript α implies that we look at the mean field evolving in the presence of a Rydberg impurity in the state $|\alpha\rangle$. Inserting (5) into (12), we can reach for short times

$$\phi_\alpha(\mathbf{x}, t) = \phi_0(\mathbf{x}) + \sum_{\mathbf{q}}[u_{\mathbf{q}}(\mathbf{x})d_{\mathbf{q}}(-i\omega_{\mathbf{q}}t) - v_{\mathbf{q}}^*(\mathbf{x})d_{\mathbf{q}}(i\omega_{\mathbf{q}}t)]$$
$$+ \alpha\sum_{\mathbf{q}}\frac{\Delta\kappa_{\mathbf{q}}^{-}}{\hbar\omega_{\mathbf{q}}} \times [u_{\mathbf{q}}(\mathbf{x})(-i\omega_{\mathbf{q}}t) - v_{\mathbf{q}}^*(\mathbf{x})(i\omega_{\mathbf{q}}t)]. \quad (13)$$

Converting the sum $\sum_{\mathbf{q}}$ into a continuum integration using $\sum_{\mathbf{q}} \to \int d^3\mathbf{q}\frac{\mathcal{V}}{(2\pi)^3}$ as usual, we can simplify this to

$$\phi_\alpha(\mathbf{x}, t) = \sqrt{\rho} - it\frac{g_0}{\hbar}\sqrt{\rho}\left|\psi^{(\alpha)}(\mathbf{x})\right|^2(\bar{u}_{\mathbf{q}}^2 - \bar{v}_{\mathbf{q}}^2), \quad (14)$$

which coincides with (10), since $\bar{u}_{\mathbf{q}}^2 - \bar{v}_{\mathbf{q}}^2 = 1$. Thus, the time evolution of Bogoliubov operators in the SBM reproduces the

same mean-field evolution as the GPE for a Rydberg impurity in a specific quantum state. We numerically verified this in the inset of Fig. 2(b), using the high-level language XMDS [56,57]. The agreement confirms the BdG model underlying (1), since coherent processes due to higher-order phonon operators are included in the GPE, but do not yet cause a visible deviation compared to the SBM.

We have thus established the intuitive picture of coherence tied to the overlap of mean-field wave functions and provided a practical method to evaluate $r(t)$ in Eq. (9). Beyond the present context, the latter can provide a useful way for calculating other internal impurity decoherence times, e.g., for ions [58], as long as impurity BEC interactions are amenable to mean-field theory. We verify in Refs. [54,59] that they are in our case, and hence the product ansatz for $|\Psi_\alpha\rangle$ should provide a good approximation.

Imaging the qubit environment interface. Entanglement between the system and environment is responsible for decoherence and is encoded in the total state. For our main result, we now show that the Rydberg-BEC realization of a qubit and environment can provide unique access to the mesoscopically entangled state $|\Psi_{\rm tot}(t)\rangle$ in Eq. (3) by inspection of the environment. To this end, the experiment must first move the entanglement of the system-environment into the environment only. This can be done by a fast $\pi/2$ microwave pulse that maps $|\downarrow\rangle \to (|\downarrow\rangle - i|\uparrow\rangle)/\sqrt{2}$ and $|\uparrow\rangle \to (|\uparrow\rangle - i|\downarrow\rangle)/\sqrt{2}$, leaving the state (3) with $c_s = 1/\sqrt{2}$ in

$$|\Psi_{\rm tot}\rangle = \tfrac{1}{2}[|\uparrow\rangle(|\Psi_\uparrow\rangle - i|\Psi_\downarrow\rangle) - i|\downarrow\rangle(|\Psi_\uparrow\rangle + i|\Psi_\downarrow\rangle)]. \quad (15)$$

A subsequent projective measurement of the Rydberg state with standard techniques, and selecting results with $|\uparrow\rangle$ then results in a mesoscopic environmental superposition state $|\Psi_{\rm ms}(t)\rangle \sim A[|\Psi_\uparrow(t)\rangle - i|\Psi_\downarrow(t)\rangle]$, where $A = 1/\sqrt{2(1+{\rm Im}[\langle\Psi_\uparrow(t)|\Psi_\downarrow(t)\rangle]}$ normalizes the many-body wave function. This state shows characteristic features in the corresponding total density $\varrho_{\rm ms}(\mathbf{r}) = N\int d^3\mathbf{x}_2\cdots\int d^3\mathbf{x}_N|\Psi_{\rm ms}(\mathbf{r},\mathbf{x}_2,\ldots,\mathbf{x}_N)|^2$, where $\Psi_{\rm ms}(\mathbf{x}_1,\mathbf{x}_2,\ldots,\mathbf{x}_N) = \langle\mathbf{X}|\Psi_{\rm ms}\rangle$ is the position-space representation of the many-body state.

To extract these features, we take the difference $\Delta\varrho(\mathbf{r}) = \varrho_{\rm ms}(\mathbf{r}) - \varrho_{\rm inc}(\mathbf{r})$ compared to the incoherent total density $\varrho_{\rm inc}(\mathbf{r}) = (\varrho_\uparrow + \varrho_\downarrow)/2$, where $\varrho_\uparrow$ ($\varrho_\downarrow$) is the total density in the presence of spin $|\uparrow\rangle$ ($|\downarrow\rangle$), e.g., $\varrho_\uparrow = |\phi_{\alpha=\uparrow}(\mathbf{r})|^2$ resulting from Eq. (8). $\varrho_{\rm inc}$ can be found in an experiment when measuring the density in state (3) directly, ignoring the spin and thus effectively averaging over it. Importantly, the total density in a mesoscopic superposition state is different by

$$\Delta\varrho(\mathbf{r}) = \left(A^2 - \frac{1}{2}\right)(\varrho_\uparrow + \varrho_\downarrow) - iA^2\left(N\frac{\varphi_\uparrow^*(\mathbf{r})\varphi_\downarrow(\mathbf{r})}{\int d^3\mathbf{x}\varphi_\uparrow^*(\mathbf{x})\varphi_\downarrow(\mathbf{x})}r(t) - \text{c.c.}\right). \quad (16)$$

Clearly, $\Delta\varrho(\mathbf{r})$ is directly related to $r(t)$.

We assess the observability of this signal in Fig. 2, showing the column densities $\overline{\Delta\varrho}(x,z) = \int dy\Delta\varrho(\mathbf{r})$ and $\overline{\varrho_{\rm inc}}(x,z) = \int dy\varrho_{\rm inc}(\mathbf{r})$ relevant for experiments, with the quantization axis along z. In the inset we show the maximum $s(t)$ of $\overline{\Delta\varrho}$ as a red curve. The signal reaches 3% of the bulk value, which should be accessible using high-sensitivity density measurements [60] or electron microscopy [61]. It is transient, since from Eq. (16) it must vanish initially and once decoherence is complete.

Thus a Rydberg qubit embedded in a condensed environment offers unique opportunities to probe the environmental origin of decoherence, through a signal heralding the transient buildup of the mesoscopically entangled state causing decoherence. Further, one could coherently manipulate the initial state of the BEC environment in order to functionalize its impact on the qubit or investigate decoherence-free subspaces [62] by initializing the qubit in a superposition $(|\nu(l=1,m=1)\rangle + |\nu(l=1,m=-1)\rangle)/\sqrt{2}$.

Being able to image the interface to the environment distinguishes the proposed setup from other open quantum systems where the environment is initially in a thermal state or not all of its degrees of freedom can be imaged simultaneously. At later times, the nonequilibrium dynamics for which we consider only the onset here results in the formation of polarons [10,63–67], with many-body correlations that go beyond the methods employed here. Nonetheless also in that case Eq. (3) holds, and coherence measurements combined with a modified signature $\Delta\varrho(\mathbf{r})$ can provide an additional experimental handle on polaron formation, not possible for embedded spins in electronic ground states [18–27,68–70].

Microwave-driven Rydberg impurity. For the predictability of the signature in Fig. 2, the block structure in $\hat{H}_{\rm tot}$ was essential. To demonstrate that moving beyond this the platform can push the frontier of our understanding of how many-body quantum dynamics gives rise to decoherence, we now tackle $\Omega_{\rm mw} \neq 0$, removing that block structure, such that the signal $\Delta\varrho(\mathbf{r})$ is no longer straightforwardly predictable, but advanced numerical techniques such as bosonic density functional theory (DFT) [71] or the multilayer multiconfiguration time-dependent Hartree method for bosons (ML-MCTDHB) [72,73] would be required and challenged.

For now we focus on the qubit side in this complex scenario only, which permits the use of a computational technique for open quantum systems, namely non-Markovian quantum state diffusion (NMQSD) [74] solved through the hierarchy of pure states (HOPS) [75]. The method is relatively fast and gives reliable results for the SBM over a large range of parameters [76]. The required system Hamiltonian $\hat{H}_{\rm syst}$ is given in (1), where now Δ has become the microwave detuning. The environmental correlation functions $C(\tau)$ have been determined in Ref. [39], and an example is shown in the inset of Fig. 3(a). As required for HOPS, we use the method of Ref. [77] to fit the correlation function with a sum of M damped oscillations

$$C(\tau) = \sum_{j=0}^{M-1} g_j e^{-(i\Omega_j+\gamma_j)\tau}, \quad (17)$$

where g_j is the weight of each exponential and Ω_j and γ_j their frequencies and damping rates. The quantum-many-body evolution is found through a stochastic wave-function hierarchy $f^{(\mathbf{k})}$, where $\mathbf{k}$ is a vector valued hierarchy index, with one component k_j for each term in the representation of the bath correlation function. Only the zeroth order $f^{(\mathbf{0})} = f^{(0,\ldots,0)}$ of the wave-function hierarchy is used to calculate expectation values of system operators using $\langle\hat{O}\rangle = \langle f^{(\mathbf{0})}|\hat{O}|f^{(\mathbf{0})}\rangle$. Its time

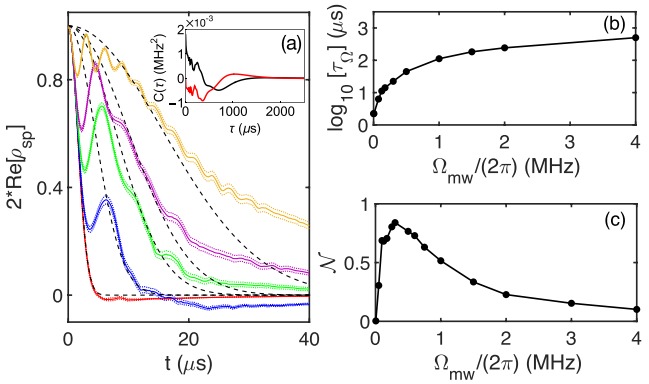

FIG. 3. Non-Markovian Rydberg decoherence dynamics. (a) Coherence between states $|s\rangle$ and $|p\rangle$ at $\nu = 120$ as a function of time for increasing resonant ($\Delta = 0$) microwave coupling strengths $\Omega_{\rm mw}$ and initial state $|+\rangle$. From top to bottom, $\Omega_{\rm mw}/(2\pi) = (0.3, 0.175, 0.125, 0.075, 0.005)$ MHz. The black dashed lines show a fit of $\rho_{sp} = \rho_{sp}(0)\exp[-(t/\tau_\Omega)^2]$. The inset shows the bath correlation function Re$[C(\tau)]$ (black) and Im$[C(\tau)]$ (ref) from Eq. (17) for $\nu = 120$, calculated as in Ref. [39]. (b) Decoherence times τ_Ω from fits as in (a) as a function of microwave strength $\Omega_{\rm mw}$. (c) Estimated non-Markovianity $\mathcal{N}$ based on the net increase of trace distances between selected system states. We use 1000 stochastic trajectories.

evolution is however coupled to all higher levels according to

$$\frac{\partial}{\partial t} f^{(\mathbf{k})}(t) = \left[-i\hat{H}_{\rm syst}(t) - \mathbf{k}\cdot\mathbf{w} + \hat{L}\tilde{z}_t\right] f^{(\mathbf{k})}(t) + \sum_j k_j g_j f^{(\mathbf{k}-\mathbf{e}_j)}(t) - \sum_j \hat{L}^\dagger f^{(\mathbf{k}+\mathbf{e}_j)}(t), \quad (18)$$

where $\mathbf{w} = [w_1, \ldots w_M]^T$, with $w_j = i\Omega_j + \gamma_j$ [see Eq. (17)]. Further, $\hat{L}$ is the system part of the coupling term to the environment, which is $\hat{L} = \sigma_z$ in Eq. (1) and $\mathbf{e}_j$ is a unit vector along the Cartesian direction j. The system-environment coupling enters (18) twofold, through $\hat{L} = \hat{\sigma}_z$ and through the shifted noise $\tilde{z}_t$, with

$$\tilde{z}_t = z_t^* + \int_0^t ds\, C^*(t-s)\langle\hat{L}^\dagger\rangle, \quad (19)$$

where $\langle\cdot\rangle$ denotes the normalized average over $f^{(0)}$. The unshifted noises z_t^* are constructed such that their temporal correlation function is exactly the bath correlation function,

$$\overline{z_t z_s^*} = C(t-s), \quad (20)$$

where $\overline{\cdots}$ denotes the stochastic average.

When the qubit is driven, we find very clear characteristic non-Markovian features in the decoherence dynamics, shown in Fig. 3(a). Instead of a monotonic decay of coherence, there are partial revivals or oscillations. Intuitively, the impurity excites sound waves in the condensate that can impact back on it at a later time [21] due to long-range interactions. We extract the overall initial decoherence times τ_Ω from Gaussian fits indicated by dashed lines in Fig. 3(a) and show them in Fig. 3(b). Clearly the decoherence time is tunable through $\Omega_{\rm mw}$, in addition to ν discussed before.

Finally, we compare the degree of non-Markovianity $\mathcal{N}$ for different parameters using the measure developed by Breuer *et al.* [78,79], an estimate of which we show in Fig. 3(c). To quantify the degree of non-Markovinity, we thus consider two different initial system density matrices $\hat{\rho} = |s\rangle\langle s|$ and $\hat{\rho} = |p\rangle\langle p|$, and monitor how the trace distance between the two states evolves in time. Non-Markovinity can be quantified by integrating positive rates of change over time [78]. The result is shown in Fig. 3(c). It is clear that the non-Markovianity of the system depends on the microwave strength. It was expected that the system behaves non-Markovian, since its characteristic timescales (for Rydberg systems $\sim\mu$s) are much shorter than the environmental memory time $T_m \approx 2000\,\mu$s for $\nu = 120$, set by the relevant phonon frequencies $\omega_{\mathbf{q}} \sim 5$ kHz. T_m decreases for smaller ν and reaches $T_m = 17\,\mu$s at $\nu = 30$, but still is only slightly shorter than the Rydberg lifetime, which limits system evolution times. Rydberg qubit decoherence will thus generally remain non-Markovian.

In the non-Markovian regime just discussed, imaging the qubit to environment interface can give insights on the back and forth flow of information between the two [78], provide hints on how to shield qubits from decoherence [62], and challenge advanced quantum-many-body methods [71,72]. Even more environment interrogation techniques are available in BEC, such as precision phonon spectroscopy [30]. The non-Markovianity $\mathcal{N}$ itself is experimentally accessible when also measuring qubit coherence with Ramsey spectroscopy.

The approach demonstrated in this section also completes the toolkit required for a comprehensive treatment of Rydberg impurities in BEC. For example, NMQSD allowed us to verify that phonon-induced Rydberg transitions, which would give rise to terms $\sim\hat{\sigma}_y \otimes (\tilde{b}_{\mathbf{q}} + \tilde{b}_{\mathbf{q}}^\dagger)$ in the Hamiltonian [39], are strongly suppressed by the energy mismatch between ΔE and $\hbar\omega_{\mathbf{q}}$ and hence neglected in Eq. (1) here.

Conclusions and outlook. We propose that the interface between a qubit and its environment can be imaged, if the former is realized by a Rydberg atom and the latter by an embedding BEC. This opens up an experimental window on both intertwined aspects of decoherence, spin and environment, evolving into a mesoscopic superposition state such as (3). Experimentally probing the interface through straightforward column densities could test the foundations of open quantum systems, provide insights on the environmental side of decoherence that suggest avenues for its mitigation, and benchmark the most advanced numerical many-body techniques.

This is possible since the Rydberg atom, in a superposition of electronic states, acts as the control handle that can affect the BEC environment over an optically resolvable range of micrometers and as a probe that is itself straightforward to read out. Neither of these advantages holds for embedded spins in electronic ground states [18–27,68–70]. For Rydberg impurities, we demonstrate that the timescale where the target signal exists can be tuned from the order of nanoseconds to microseconds by the choice of the excited Rydberg principal quantum number ν or additional microwave driving.

Acknowledgments. We gladly acknowledge fruitful discussions with Rick Mukherjee and Swagata Mallick, and thank the Science and Engineering Research Board (SERB), Department of Science and Technology (DST), New Delhi, India, for financial support under research Project No. EMR/2016/005462, and the Max-Planck society under

the MPG-IISER partner group program. R.N. acknowledges support from a UKIERI-UGC Thematic Partnership No. IND/CONT/G/16-17/73 UKIERI-UGC project and DST-SERB for the Swarnajayanti fellowship File No. SB/SJF/2020-21/19. A.E. acknowledges support from the DFG via a Heisenberg fellowship (Grant No. EI 872/5-1).

[1] M. A. Schlosshauer, *Decoherence: And the Quantum-to-Classical Transition* (Springer, Berlin, 2007).
[2] M. Schlosshauer, Rev. Mod. Phys. **76**, 1267 (2005).
[3] J. F. Poyatos, J. I. Cirac, and P. Zoller, Phys. Rev. Lett. **77**, 4728 (1996).
[4] F. Verstraete, M. M. Wolf, and J. Ignacio Cirac, Nat. Phys. **5**, 633 (2009).
[5] S. L. Vuglar, D. V. Zhdanov, R. Cabrera, T. Seideman, C. Jarzynski, and D. I. Bondar, Phys. Rev. Lett. **120**, 230404 (2018).
[6] R. Heidemann, U. Raitzsch, V. Bendkowsky, B. Butscher, R. Löw, and T. Pfau, Phys. Rev. Lett. **100**, 033601 (2008).
[7] J. B. Balewski, A. T. Krupp, A. Gaj, D. Peter, H. P. Büchler, R. Löw, S. Hofferberth, and T. Pfau, Nature (London) **502**, 664 (2013).
[8] A. Gaj, A. T. Krupp, J. B. Balewski, R. Löw, S. Hofferberth, and T. Pfau, Nat. Commun. **5**, 4546 (2014).
[9] M. Schlagmüller, T. C. Liebisch, H. Nguyen, G. Lochead, F. Engel, F. Böttcher, K. M. Westphal, K. S. Kleinbach, R. Löw, S. Hofferberth, T. Pfau, J. Perez-Rios, and C. H. Greene, Phys. Rev. Lett. **116**, 053001 (2016).
[10] F. Camargo, R. Schmidt, J. D. Whalen, R. Ding, G. Woehl, S. Yoshida, J. Burgdörfer, F. B. Dunning, H. R. Sadeghpour, E. Demler, and T. C. Killian, Phys. Rev. Lett. **120**, 083401 (2018).
[11] T. Dieterle, M. Berngruber, C. Hölzl, R. Löw, K. Jachymski, T. Pfau, and F. Meinert, Phys. Rev. A **102**, 041301(R) (2020).
[12] S. Middelkamp, I. Lesanovsky, and P. Schmelcher, Phys. Rev. A **76**, 022507 (2007).
[13] J. D. Whalen, F. Camargo, R. Ding, T. C. Killian, F. B. Dunning, J. Pérez-Ríos, S. Yoshida, and J. Burgdörfer, Phys. Rev. A **96**, 042702 (2017).
[14] S. K. Kanungo, J. D. Whalen, Y. Lu, T. C. Killian, F. B. Dunning, S. Yoshida, and J. Burgdörfer, Phys. Rev. A **102**, 063317 (2020).
[15] T. F. Gallagher, *Rydberg Atoms* (Cambridge University Press, Cambridge, U.K., 1994).
[16] R. Löw, H. Weimer, J. Nipper, J. B. Balewski, B. Butscher, H. P. Büchler, and T. Pfau, J. Phys. B: At., Mol. Opt. Phys. **45**, 113001 (2012).
[17] C. J. Pethik and H. Smith, *Bose-Einstein Condensation in Dilute Gases* (Cambridge University Press, Cambridge, U.K., 2002).
[18] F. Schmidt, D. Mayer, Q. Bouton, D. Adam, T. Lausch, N. Spethmann, and A. Widera, Phys. Rev. Lett. **121**, 130403 (2018).
[19] F. Schmidt, D. Mayer, T. Lausch, D. Adam, Q. Bouton, M. Hohmann, F. Kindermann, J. Koch, J. Nettersheim, and A. Widera, Phys. Status Solidi B **256**, 1800710 (2019).
[20] Y.-J. Song and L.-M. Kuang, Ann. Phys. **531**, 1800423 (2019).
[21] P. Ostmann and W. T. Strunz, arXiv:1707.05257.
[22] S. McEndoo, P. Haikka, G. De Chiara, G. Palma, and S. Maniscalco, Europhys. Lett. **101**, 60005 (2013).
[23] A. Klein, M. Bruderer, S. R. Clark, and D. Jaksch, New J. Phys. **9**, 411 (2007).
[24] M. Cirone, G. De Chiara, G. Palma, and A. Recati, New J. Phys. **11**, 103055 (2009).
[25] M. Bruderer, A. Klein, S. R. Clark, and D. Jaksch, Phys. Rev. A **76**, 011605(R) (2007).
[26] M. Bruderer, A. Klein, S. R. Clark, and D. Jaksch, New J. Phys. **10**, 033015 (2008).
[27] M. Bruderer and D. Jaksch, New J. Phys. **8**, 87 (2006).
[28] P. Haikka, S. McEndoo, and S. Maniscalco, Phys. Rev. A **87**, 012127 (2013).
[29] I. E. Mazets, G. Kurizki, N. Katz, and N. Davidson, Phys. Rev. Lett. **94**, 190403 (2005).
[30] N. Katz, R. Ozeri, J. Steinhauer, N. Davidson, C. Tozzo, and F. Dalfovo, Phys. Rev. Lett. **93**, 220403 (2004).
[31] M. Brune, J. Bernu, C. Guerlin, S. Deléglise, C. Sayrin, S. Gleyzes, S. Kuhr, I. Dotsenko, J. M. Raimond, and S. Haroche, Phys. Rev. Lett. **101**, 240402 (2008).
[32] S. Gleyzes, S. Kuhr, C. Guerlin, J. Bernu, S. Deléglise, U. B. Hoff, M. Brune, J.-M. Raimond, and S. Haroche, Nature (London) **446**, 297 (2007).
[33] S. Deléglise, I. Dotsenko, C. Sayrin, J. Bernu, J.-M. Raimond, and S. Haroche, Nature (London) **455**, 510 (2008).
[34] R. Mukherjee, C. Ates, W. Li, and S. Wüster, Phys. Rev. Lett. **115**, 040401 (2015).
[35] T. Karpiuk, M. Brewczyk, K. Rążewski, A. Gaj, J. B. Balewski, A. T. Krupp, M. Schlagmüller, R. Löw, S. Hofferberth, and T. Pfau, New J. Phys. **17**, 053046 (2015).
[36] R. Mukherjee, T. C. Killian, and K. R. A. Hazzard, Phys. Rev. A **94**, 053422 (2016).
[37] A. Arias, G. Lochead, T. M. Wintermantel, S. Helmrich, and S. Whitlock, Phys. Rev. Lett. **122**, 053601 (2019).
[38] E. K. Dietsche, A. Larrouy, S. Haroche, J. M. Raimond, M. Brune, and S. Gleyzes, Nat. Phys. **15**, 326 (2019).
[39] S. Rammohan, A. K. Chauhan, R. Nath, A. Eisfeld, and S. Wüster, Phys. Rev. A **103**, 063307 (2021).
[40] H.-P. Breuer and F. Petruccione, *The Theory of Open Quantum Systems* (Oxford University Press, Oxford, U.K., 2002).
[41] A. J. Leggett, S. Chakravarty, A. T. Dorsey, M. P. A. Fisher, A. Garg, and W. Zwerger, Rev. Mod. Phys. **59**, 1 (1987).
[42] I. Wilson-Rae and A. Imamoğlu, Phys. Rev. B **65**, 235311 (2002).
[43] D. Xu and K. Schulten, Chem. Phys. **182**, 91 (1994).
[44] J. Leppäkangas, J. Braumüller, M. Hauck, J.-M. Reiner, I. Schwenk, S. Zanker, L. Fritz, A. V. Ustinov, M. Weides, and M. Marthaler, Phys. Rev. A **97**, 052321 (2018).
[45] A. Omont, J. Phys. **38**, 1343 (1977).
[46] We consider a homogeneous condensate with density $\rho = 9.8 \times 10^{18}$ m^{-3}, $U_0 = 4\pi\hbar^2 a_s/m$ with scattering length $a_s = 6.45$ nm and $m = 1.393 \times 10^{-25}$ kg, $g_0 = 2\pi\hbar^2 a_e/m_e$ with electron mass m_e, and electron-atom scattering length $a_e = -18a_0$ nm, all corresponding to strontium ^{84}Sr.

[47] I. I. Beterov, I. I. Ryabtsev, D. B. Tretyakov, and V. M. Entin, Phys. Rev. A **79**, 052504 (2009).
[48] R. Howl, C. Sabín, L. Hackermüller, and I. Fuentes, J. Phys. B: At., Mol. Opt. Phys. **51**, 015303 (2017).
[49] M. W. Jack, Phys. Rev. Lett. **89**, 140402 (2002).
[50] J. Dziarmaga and K. Sacha, Phys. Rev. A **68**, 043607 (2003).
[51] A. Pendse, S. Shirol, S. Tiwari, and S. Wüster, Phys. Rev. A **102**, 053322 (2020).
[52] In Sr at density $\rho = 9.8 \times 10^{18}$ m^{-3}, we expect $\tau \approx 35$ μs for $\nu = 80$ and $\tau \approx 150$ μs for $\nu = 120$, based on Ref. [14].
[53] See Supplemental Material at http://link.aps.org/supplemental/10.1103/PhysRevA.104.L060202 for a movie of spatial signatures in superposition states.
[54] S. K. Tiwari and S. Wüster, Phys. Rev. A **99**, 043616 (2019).
[55] V. Shukla, R. Pandit, and M. Brachet, Phys. Rev. A **97**, 013627 (2018).
[56] G. R. Dennis, J. J. Hope, and M. T. Johnsson, Comput. Phys. Comm. **184**, 201 (2013).
[57] G. R. Dennis, J. J. Hope, and M. T. Johnsson, http://www.xmds.org/.
[58] L. Ratschbacher, C. Sias, L. Carcagni, J. M. Silver, C. Zipkes, and M. Köhl, Phys. Rev. Lett. **110**, 160402 (2013).
[59] S. Tiwari, F. Engel, M. Wagner, R. Schmidt, F. Meinert, and S. Wüster, arXiv:1707.05257.
[60] M. Gajdacz, A. J. Hilliard, M. A. Kristensen, P. L. Pedersen, C. Klempt, J. J. Arlt, and J. F. Sherson, Phys. Rev. Lett. **117**, 073604 (2016).
[61] B. Santra and H. Ott, J. Phys. B: At., Mol. Opt. Phys. **48**, 122001 (2015).
[62] M. Schlosshauer, Phys. Rep. **831**, 1 (2019).
[63] K. K. Nielsen, L. P. Ardila, G. M. Bruun, and T. Pohl, New J. Phys. **21**, 043014 (2019).
[64] M. G. Skou, T. G. Skov, N. B. Jørgensen, K. K. Nielsen, A. Camacho-Guardian, T. Pohl, G. M. Bruun, and J. J. Arlt, Nat. Phys. **17**, 731 (2021).
[65] R. Schmidt, J. D. Whalen, R. Ding, F. Camargo, G. Woehl, S. Yoshida, J. Burgdörfer, F. B. Dunning, E. Demler, H. R. Sadeghpour, and T. C. Killian, Phys. Rev. A **97**, 022707 (2018).
[66] R. Schmidt, H. R. Sadeghpour, and E. Demler, Phys. Rev. Lett. **116**, 105302 (2016).
[67] F. Camargo, Ph.D. thesis, Rice University, 2017.
[68] H. T. Ng and S. Bose, Phys. Rev. A **78**, 023610 (2008).
[69] Y. Han, Z. Li, and L.-M. Kuang, Commun. Theor. Phys. **72**, 095102 (2020).
[70] Z. Li and L.-M. Kuang, Quantum Inf. Process. **19**, 188 (2020).
[71] C. L. Benavides-Riveros, J. Wolff, M. A. L. Marques, and C. Schilling, Phys. Rev. Lett. **124**, 180603 (2020).
[72] S. Krönke, L. Cao, O. Vendrell, and P. Schmelcher, New J. Phys. **15**, 063018 (2013).
[73] R. Schmitz, S. Krönke, L. Cao, and P. Schmelcher, Phys. Rev. A **88**, 043601 (2013).
[74] L. Diósi, N. Gisin, and W. T. Strunz, Phys. Rev. A **58**, 1699 (1998).
[75] D. Suess, A. Eisfeld, and W. T. Strunz, Phys. Rev. Lett. **113**, 150403 (2014).
[76] R. Hartmann and W. T. Strunz, J. Chem. Theory Comput. **13**, 5834 (2017).
[77] G. Ritschel and A. Eisfeld, J. Chem. Phys. **141**, 094101 (2014).
[78] H.-P. Breuer, E.-M. Laine, and J. Piilo, Phys. Rev. Lett. **103**, 210401 (2009).
[79] M. Genkin, D. W. Schönleber, S. Wüster, and A. Eisfeld, J. Phys. B: At., Mol. Opt. Phys. **49**, 134001 (2016).